

Multibody interactions lead to conformational selection of an open state in warm GABA_A receptors

Sruthi Murlidaran,^{†,‡} Reza Salari,^{†,‡,‡} and Grace Brannigan^{*,†,‡}

[†]*Department of Physics, Rutgers University, Camden, NJ, USA*

[‡]*Rutgers University, Center for Computational and Integrative Biology, Rutgers University, Camden, NJ, USA*

E-mail: i.k.groupleader@unknown.uu

Abstract

γ_2 GABAA receptors are critical for proper transmission of inhibitory signals in the central nervous system, and are common targets of anesthetic and anxiolytic drugs. They are also members of the widely-studied pentameric ligand-gated ion channel family (pLGIC). Here we use a slightly increased temperature to, for the first time, observe a stable spontaneous opening event of a pLGIC in molecular simulation. We find the opening event reflects interactions in two rings of homologous charges in the receptor transmembrane domain, an "interfacial band" containing five basic residues at M2 24' in the M2-M3 loop, and the "pore oscillator" composed of two acidic residues and one basic residue at 20' on the two β and one γ M2 helices respectively. The pore oscillator is shown to drive fluctuations in pore radius, by switching between attractive and repulsive cross-pore electrostatic interactions, consistent with a classic Coulomb charge-dipole arrangement. A conformational change of the interfacial band from an

asymmetric to a symmetric state locks the pore oscillator in a repulsive (open) configuration. The γ_2 K289M mutation is a rare mutation (rs121909672) that causes seizures with fever and also neutralizes the γ_2 residue in the interfacial band. The electrostatic energy of an interfacial band with only four charges is shown to be more sensitive to random shape fluctuations, which increase with higher temperature. Our simulation results indicate these effects are also transmitted to the pore. Temperature-enhanced fluctuations could thus cause rapid gating in these mutant receptors, consistent with flickering observed previously in single-channel recordings.

GABA(A) receptors are neurotransmitter receptors that inhibit electrical signals in the brain and are necessary to prevent seizures. They are also targets of inhibitory drugs, like sedatives and general anesthetics. Some GABA(A) mutations increase the likelihood of seizures, but only with fever, and can be found in humans. We use Molecular Dynamics Simulations to explore the effects of temperature and one such mutation on virtual GABA(A) receptors, and newly identify a set of interactions that both allows gating of Wild-type receptors and mediates the temperature effects of the mutation. This opens new doors for interpreting complex experimental results, predicting effects of amino-acid sequence on GABA(A) receptor function and other proteins in the same family, and design of anti-convulsant drugs.

Introduction

Gamma-aminobutyric acid (GABA_AR) receptors are inhibitory ionotropic receptors, critical to proper function of the mammalian central nervous system (CNS) and targets of numerous drugs aiming to depress CNS activity, such as benzodiazepines,¹ and inhalational and intravenous general anesthetics.^{2–4} They are members of the well-studied family of pentameric ligand-gated channels (pLGICs), which includes several other receptors common to CNS membranes, such as the nicotinic acetylcholine receptor (nAChR), 5HT-3 receptor, and glycine receptor. The larger family is found in a range of organisms, including

prokaryotes, and exhibits high sequence and function diversity. Surprisingly, high resolution x-ray structures have revealed a common structure that is extremely well-conserved across the family,^{5–14} which has made it particularly challenging to identify a universal group of interactions that drive gating.

Molecular simulation is a powerful technique for identifying subtle differences in interactions. It has been unfeasible to directly observe transitions to stable open states even in long molecular simulations of pLGICs, and pLGIC open state structures reliably close upon unbiased simulation, even under conditions in which they're expected to be stable.^{15–18} Identifying opening pathways, therefore, requires an artificial bias or selection process to drive the receptor toward an open conformation. The pH-sensitive prokaryotic pentameric GLIC channel has been crystallized at high resolution in multiple conformations, and at pH corresponding to both resting and active states;^{9–11} probable pathways between conformations have been determined using increasingly sophisticated molecular dynamics algorithms.^{19–22} Such studies have identified collective motions common to the gating pathway, with Lev et al²² recently identifying a sequence of collective events common to pathways generated using an enhanced sampling technique known as the string method.

The underlying origins of this instability have not been identified despite extensive efforts, in part because identifying the essential interactions missing from the simulation requires answering *a priori* the primary question the simulations hope to address : which interactions drive pore opening and closing. Simulations of gating in neurotransmitter-gated pLGICs are further hampered by low orthosteric ligand binding affinity due to a loss of cation-π interactions in non-polarizable forcefields.

Here we circumvent both these obstacles by exploiting the allosteric properties of pLGICs. In a classic Monod-Wyman-Changeux^{23,24} model of allostery, unliganded receptors still fluctuate between active and resting conformations, with the probability of the active conformation usually expected to increase with small temperature increases. We observe conformational shifts consistent with the events at the domain interface reported by Lev et al,²² but

are able to further identify the sequence of events preceding the spontaneous pore opening, as well as the collective electrostatic interactions that drive them.

Each pLGIC subunit consists of an extracellular agonist-binding domain (ECD) and a transmembrane domain (TMD) containing a four helix bundle with helices labeled (M1-M4). The M2 helices line the pore, and the M2-M3 loop connecting the M2 and M3 helices interacts directly with both the TMD and the ECD. The loop has long been hypothesized to transmit agonist binding to the transmembrane domain,²⁵⁻³⁰ with several mutation studies indicating the importance for agonist sensitivity of attractive electrostatic interactions among contact residues, such as salt-bridges, between the M2-M3 loop and the ECD.³¹⁻³⁴ The mechanism through which a change in these salt bridges (either forming or breaking) opens the pore is still unclear.

Our results suggest a non-specific mechanism for the final steps of gating that relies on multibody interactions within two sets of homologous charged residues: 1) a group of three residues containing both positive and negative charges, facing into the pore and forming a rapidly oscillating charge-dipole arrangement, which we term the pore oscillator, and 2) an interfacial band of five like charge residues at the interface of the ECD and TMD which, upon an energetically unfavorable conformational change, selects for an open conformation of the pore oscillator(Figure 1).

We show using simple electrostatic expressions that repeated cross-pore repulsions in the interfacial band introduce a significant energetic penalty for shrinking the interfacial band, and that the symmetry inherent in the interfacial band amplifies the interactions between distant residues. Molecular dynamics simulations indicate this repulsion among interfacial band residues can be propagated along M2 helices to open the hydrophobic gate. In GABA_AR receptors, the interfacial band is formed by a basic residue in the M2-M3 loop conserved across GABA_AR subunits as $\alpha K279$, $\beta K274$, or $\gamma K289$ (Figure 1), and notated as M2 24' in the prime numbering scheme suggested in.³⁵ Sequence conservation of these charges across GABA_AR subspecies is shown in Figure S3. M2 24' has been previously shown to be

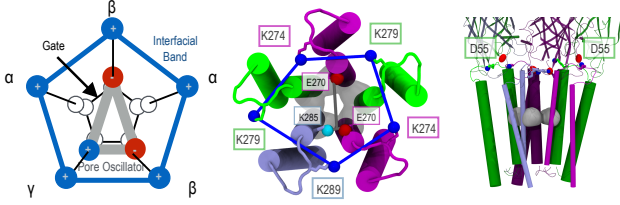


Figure 1: (A) Schematic of the GABA_{AR} pore with relevant multibody interactions. A conserved basic residue at 24' in the M2-M3 loop forms a pentamer of positive charges, interfacial band, drawn here in blue. The γ K289M mutation neutralizes one of the charges. One turn closer to the intracellular domain, one basic residue and two acidic residues constitute a charge-dipole arrangement, pore oscillator, is shown in gray. The tightest constriction is at the hydrophobic gate at 9', lined by five leucines (white). (B) View of the TMD from ECD, colored by subunit; γ - iceblue; β - purple; α - green. Charged ends of the residues forming the interfacial band and pore oscillator are represented by spheres connected (for visualization only) by gray and blue bonds respectively. Space-filling representation in gray depicts the hydrophobic gate at 9'. (C) Side view of ECD and TMD showing the residues in (B), as well as the position of α D55 in the ECD.

critical for conferring sensitivity to agonist; Harrison and colleagues³³ demonstrated via shift in EC50 that charge-reversal of α 279 reduced sensitivity, which was restorable via additional charge-reversal of α D57 or α D149, both within the ECD and in the vicinity of the M2-M3 loop. Similar behavior was observed in the nicotinic acetylcholine receptor (nAChR), upon charge-reversal of α R209 in M1 and α E45 in the ECD.²⁸

The basic residue at M2 24' is also conserved in GLIC, ELIC, and GlyR, and was further implicated in interdomain communication in simulations of GLIC by Lev et al,²² who also found that salt bridging of M2 24' with the ECD (D32) is correlated on a “high-probability communication pathway” with shrinking distances between M2 helices and pore closure. A causative and predictive physical mechanism, however, was not established.

Negative effects of a natural but uncommonly occurring missense single nucleotide polymorphism (SNP) at M2 24' in the γ_2 subunit supports a role for collective charge interactions in stabilizing the open state. The γ_2 :K289M mutation has been reported in families with generalized epilepsy and febrile seizures plus(GEFS+),³⁶⁻³⁸ a generalized phenotype that often includes only febrile (fever-caused) seizures until about age 11, but can also include less severe myoclonic, atonic, or absence seizures at normal body temperature. In $\alpha_1\beta_2\gamma_2$

K289M receptors, GABA-evoked current amplitude was dramatically reduced relative to the WT,^{37,39} while in $\alpha_1\beta_3\gamma_2$ K289M receptors the mutation did not affect current amplitudes but did increase the deactivation rate.⁴⁰ In the latter receptors, currents had reduced mean open times, in part due to flickering.^{34,38,41} In hippocampal neurons containing GABA_AR with γ_2 :K289M subunits, accelerated desensitization of inhibitory post synaptic currents was also observed.⁴⁰ Although a mechanism involving reduced trafficking has been proposed,⁴² this would not explain the flickering observed in single-channel recordings.³⁸

We have run unbiased MD simulations and adaptive biasing force (ABF) calculations of the $\gamma K289M$ mutant at multiple temperatures, and detect occluded channels at higher temperatures consistent with the known behavior of the K289M mutants, with differential dynamics of the interfacial band consistent with expectations based on the multibody expression. We propose a mechanism underlying the mutation's effects, involving destabilization of the open state due to the reduced cost to shrink a interfacial band with significant shape fluctuations .

MATERIALS AND METHODS

Simulations

This manuscript considers data from four systems: two replicas of the wildtype $\alpha_1\beta_1\gamma_2$ receptor (termed K1, K2) and 2 replicas of the K289M mutant (M1, M2). Each system was run for 500 ns at both 300K and 315K, for a total of 4 μs of unbiased MD simulation. Additional free energy calculations involved the K1 and M1 systems. The model used in this paper corresponds to Model 1 - CHOL from Reference,⁴³ and was built with GluCl (PDB code : 3RHW) as a template as well as the alignments published in Ref.⁴⁴ Further justification and details on this model can be found in Reference.⁴³ The systems were prepared as in Ref,⁴³ by embedding the protein in a homogenous lipid bilayer composed of phosphatidylcholine (POPC) built using CHARMM Membrane builder, with the final system containing 266

POPC molecules. All simulations used the CHARMM22-CMAP⁴⁵ force field with torsional corrections for proteins. The CHARMM36 model^{46,47} was used for phospholipids, ions, water and cholesterol molecules. Energy minimization and MD simulations were conducted using the NAMD2.9 package.⁴⁸ A cutoff of 1.2 nm was used for non-bonded potentials, with a switching function starting at 1.0 nm; all simulations employed periodic boundary conditions, and long-ranged electrostatics were handled with smooth Particle Mesh Ewald method with a grid spacing of approximately 1Å. All simulations were run in the NPT ensemble with weak coupling to Langevin thermostat at temperature 300 or 315K, and a Langevin barostat at 1 atm. High temperature (315K) simulations were run for 500 ns following 200 ns of simulation at the lower temperature (300K). Full details are provided in SI.

Analytical Prediction of Multibody Interactions

Our simulation analysis is motivated by the multibody interactions within two arrangements of charges found around the GABA(A)r pore, representing the interfacial band and the pore oscillator. Each arrangement includes residues on opposite sides of the pore, and the plane containing the residues is normal to the pore axis, so attractive and repulsive interactions within the arrangement will contribute directly to pore-closing and pore-opening, respectively.

Charged pentamer

As shown in SI Theory, the total Coulomb energy for a charged pentagon with average side length \bar{r} and average diagonal length \bar{s} is

$$U_{+5}(\bar{r}, \delta_\phi) = \frac{5k_e e^2 \phi}{\bar{r}} \left(1 + \frac{\delta_\phi}{\phi} \right) + O(\bar{\delta r}^2) + O(\bar{\delta s}^2) \quad (1)$$

where e is the electron charge, $k_e = 332\text{\AA}/\text{kcal/mol}/e^2$ is the Coulomb constant, and $\bar{\delta r}^2$ and $\bar{\delta s}^2$ are the variance in r and s across the five sides of the pentamer. For a regular pentamer

$\bar{s} = \phi\bar{r}$ where $\phi \equiv (1 + \sqrt{5})/2 \sim 1.62$ is a geometric constant often called the “golden ratio”, with the convenient property $1/\phi = \phi - 1 = 0.62$. δ_ϕ is the deviation of $\frac{\bar{r}}{\bar{s}}$ from the value for a regular pentamer : $\delta_\phi \equiv \frac{\bar{r}}{\bar{s}} - (\phi - 1)$.

The linear term in δ_ϕ reflects the effects of shape fluctuations on the relative contributions of diagonal and adjacent pairs. Second-order terms given by $\bar{\delta r}^2$ and $\bar{\delta s}^2$ reflect variance in the adjacent and diagonal distances respectively. According to Eq. 1, positive values of δ_ϕ (in which diagonal distances are shorter than expected in a regular pentamer) will increase the overall energy of the interfacial band, provided the average distance between adjacent residues (\bar{r}) is kept constant. This asymmetry-induced increase in energy can be offset by an overall increase in the size of the interfacial band : $\delta_\phi < 0$ will stabilize a larger \bar{r} . Similarly, negative δ_ϕ will decrease the overall energy of the interfacial band and allow it to close with reduced penalty.

Neutralizing any of the charges removes two diagonal and two adjacent interactions, so the Coulomb energy for 4 like-charges arranged on a pentagonal lattice is

$$U_{+4}(\bar{r}, \delta_\phi) = \frac{3k_e e^2 \phi}{\bar{r}} \left(1 + \frac{\delta_\phi}{\phi} \right) + O(\bar{\delta r}^2) + O(\bar{\delta s}^2) \quad (2)$$

$$= \frac{3}{5} U_{+5}(\bar{r}, \delta_\phi) \quad (3)$$

where averages only consider distances involving charged residues, and therefore \bar{r} and δ_ϕ incorporate only three adjacent distances and three diagonal distances. The factor of $3/5$ will generally stabilize a smaller value of \bar{r} at any temperature, but $\delta_\phi, \bar{\delta r}^2, \bar{\delta s}^2$ will also be directly dependent on temperature. The simple Coulomb calculation represented in Eq. 1 indicates a large energetic cost of shrinking the interfacial band over typical distances (Fig S1B). Considering typical distances between homologous residues in pLGICs, the strength of the interaction among homologous residues may be unintuitive. Reducing the distance between two like charges from $r_1 = 15\text{\AA}$ to $r_1 = 12\text{\AA}$ raises the electrostatic energy by only 5.5 kcal/mol, but shrinking the regular pentagon (including diagonal interactions) from

$r_1 = 15\text{\AA}$ to $r_1 = 12\text{\AA}$ increases the energy of the arrangement by 49 kcal/mol! Diagonal, cross-pore interactions contribute almost 20 kcal/mol, nearly doubling the total.

Charge-dipole

Farther away from the interface with the ECD, facing the pore, is another charged ring of three residues, at M2 20' (β E270 and γ K285), that we term the “pore oscillator” because it exhibits rapid shape fluctuations that are propagated to the hydrophobic gate. The Coulomb energy reflects two diagonal interactions, and one adjacent interaction, and is effectively a charge-dipole interaction:

$$U_{c-dp} = -\frac{k_e e^2}{r} \left(\frac{r}{d} + \frac{1}{z^+} - \frac{1}{z^-} \right) \quad (4)$$

$$z^\pm \equiv \sqrt{1 + \left(\frac{d}{2r} \right)^2 \pm \frac{d \cos \theta}{r}} \quad (5)$$

where U_{c-dp} is the Coulomb energy of the charge-dipole, d is the distance between the two charges forming the dipole, r is the separation between the charge and dipole midpoint, z^\pm are the distances between the charge and the close and far ends of the dipole, respectively, and θ is the angle between the dipole and dipole midpoint-charge separation vector (see diagrams in Fig. 3C and S1B).

It is common in undergraduate-level treatment of charge-dipole interactions to assume $r/d \gg 1$ in Eq. 4, but for a charge-dipole arranged on a regular pentagonal lattice, $r/d \equiv \phi \sim 1.6$. One central result from the usual treatment is that at $\theta = \pi/2$, the interaction switches from being attractive to repulsive, with a discontinuity at the boundary; this result still holds in the full expression (Fig S1B), as expected.

RESULTS AND DISCUSSION

Spontaneous opening event at 315 K

A spontaneous opening event was observed in one WT replica at the higher temperature. In this replica, the pore was closed for over 500 ns at 300K (Figure S6), but after raising the temperature to 315K and about 200 ns of simulation, a spontaneous set of events induced a stable open pore for the remainder of the simulation. (Figure 3, and SI Movie S1). The event itself took about 100-150 ns, and involved the following stages, shaded by the specified colors in Figure 3.

1. **Early (blue): Symmetrization of interfacial band.** The interfacial band begins in an elongated conformation, because the side-chain of one charged residue (α_{γ} -K279) faces away from the pore axis, while all other side-chains face toward it. Between 200 and 260 ns, this side-chain flips, causing the interfacial band to switch from an elongated to a regular conformation (Figure 2 A). This flip may be dependent upon flexibility introduced by the adjacent proline (α P278); the conservation³⁵ and significance of this proline for function²⁷ are well-established, although its fundamental role in gating has been unclear.
2. **Mid (orange): Response to symmetrization; partial opening and deformation.**
 - (a) $t = 260\text{-}300$ ns: The previous symmetrization step is electrostatically unfavorable for the other residues of the interfacial band and for the basic residue of the pore oscillator; in response, the M2 helices of the flipped α subunit and the γ and β subunit on either side separate from the other two subunits. This initiates widening of the pore, as shown by the sharp transition in Figure 2 D. Simultaneously, the positively-charged end of the pore oscillator dipole (γ -K285) is deflected toward the intracellular domain and away from the ECD (Figure 3). This destabilizes its

salt-bridge with the negatively charged residue comprising the other end of the “dipole”, β_{γ} -E270.

- (b) t=300-330 ns: Upon weakening of favorable electrostatic interactions with positively charged residues in the pore oscillator and interfacial band, the two negative sidechains of the pore oscillator pivot around their C_{α} atom to face away from the γ subunit. This switches the pore oscillator charge-dipole interaction from attractive to repulsive, as tracked by θ in Figure 3 C and according to Eq. 4; for small values of θ , the distance between the two negatively charged residues becomes particularly small (Figure 3).

3. Late (red): Recoil and Stabilization.

The pore-oscillator is now in a highly unfavorable configuration due to proximity of the two negative charges corresponding to low values of θ . The resulting repulsion causes a rapid separation of the charges. This is further propagated to increase the distance between their respective M2 helices, as indicated by an additional increase in pore radius, not just at the pore oscillator but also at the minimum constriction 16-17 Angstroms away (Figure 2 D). The trajectories of θ and the time derivative of the minimum pore constriction are shown plotted on the same axis in Figure 2 C; the two most rapid increases in the pore radius each occur directly after the two θ compression events (at t = 100 ns and t = 325 ns). This association was also qualitatively observed in the other replica trajectories (Figures S5-S11), although in some cases it was a less acute value of θ , held over a longer time period, that preceded opening.

Upon recoil, each of these two acidic residues formed an intrasubunit salt-bridge with a basic residue of the interfacial band (Figure 2 B). Since the charged interfacial band is resistant to shrinking, these salt-bridges can only form if the acidic residues in the pore oscillator are also separated. The timing of events is consistent with pore oscillator recoil simultaneously allowing salt-bridging with the interfacial band and causing

an overall separation of M2 helices. Due to the stochastic nature of the trajectory, determining the typical order of these two events would require many more replicas.

The pore oscillator samples small values of θ regardless of the configuration of the interfacial band, due to high frequency oscillations consistent with the discontinuity in the interaction, including twice in this particular trajectory (once at $t = 100\text{ ns}$ and once at $t = 350\text{ ns}$). Such events were observed in all simulated systems and were usually followed by brief opening of the pore. A stable opening event, however, was only observed when salt-bridging of each of the pairs of β -E270 and β -K274 residues was also stable, which depended upon the symmetrization step. The significance of the symmetric interfacial band is verified through the next set of simulations involving a mutant of an interfacial band residue.

γ K289M increases energetic sensitivity to shape fluctuations of the interfacial band

The multibody mechanism proposed in the previous section suggests an important role for each basic residue in the interfacial band for conferring stability of the open state, beyond communication with the agonist-binding domain. γ subunits are not required for functional GABA(A) receptors, and do not participate in the interfaces forming the orthosteric binding sites. Yet neutralizing the γ -contributed charge to the interfacial band causes flickering in single-channel recordings³⁸ and is associated with fever-induced seizures.

Simulations of the two K289M replicas at both 300K and 315K, as for the WT receptors, indicated a reverse temperature dependence for the distribution of minimum pore radii (Figure 4). As shown in Figure 4 A, we observe no effect of the mutation on the overall distribution of pore radii at 300K. At 315K, the WT distribution broadens, as expected (Figure 4 B). The K289M distribution broadens even more at the higher temperature, but is also shifted toward smaller radii, so that at 315K both WT replicas have larger pore radii than both K289M replicas for most frames.

Eq. 3 indicates three possible contributions to a reduced cost for shrinking the K289M interfacial band compared to that of the WT interfacial band:

1. The reduced charge of the K289M interfacial band results in a factor of 3/5 for the overall energetic cost to shrink the K289M interfacial band, assuming the same value of \bar{r} and δ_ϕ . This contribution is not temperature dependent, and the 40% loss is large enough that it is perhaps most surprising that an K289M receptor is functional at any temperature. This may be explained by the observation that in the K289M systems, $\gamma M220'$ (M2 K285) of the pore oscillator assumes a position much closer to the original position of K289.
2. Any reduction in δ_ϕ will destabilize the open state by reducing the energetic cost to shrink the interfacial band(Eq. 1). Both increased temperature and the loss of charge symmetry would be expected to increase the root-mean-square-displacement (RMSD) of each remaining side-chain. We ran simple numerical calculations to determine how increased RMSD in individual charges affects the distribution of δ_ϕ , shown in Figure S2. The distribution of δ_ϕ is not particularly sensitive to RMSD if all five charges of a closed pentagon are used, due to geometric constraints and the non-cohesive nature of the noise. The distribution is expected to widen with increased RMSD, but mainly in the positive direction (Figure S2A).
3. Even if each individual (conserved) charge has the same RMSD in the K289M and WT receptors, the distribution of δ_ϕ will be broadened in the K289M receptor because only three of the five adjacent and diagonal distances are used to calculate the average adjacent and diagonal distances, and they are not constrained by the requirement of forming a closed pentagon (Figure S2). Furthermore, the broadening is symmetric, with significant probability of $\delta_\phi < 0$. This is consistent with what we observe in the molecular systems, as shown by deviations of the ratio of diagonal to adjacent distances from $1/\phi$ (Figure 4 C,D) over each trajectory.

Comparison between Figure 4A,B and C,D, reveals similar trends for distributions of minimum pore radius and δ_ϕ , upon introducing the mutation, raising the temperature, or both.

The pore oscillator-interfacial band salt-bridge formation becomes uncorrelated from the pore radius in the K289M systems, as shown in Figure 4 F.

γ K289M increases barriers to conduction via channel conformation rather than direct interactions with ions

Determining whether a single ion channel conformation corresponds to an “open” or “closed” state is frequently not possible in unbiased MD simulations, except for conformations at an extremum. A Cl- atom has a radius of approximately 1.8Å, the hydrophobic residues lining the minimum pore radius but makes it unlikely a Cl- atom will pass through a constriction of exactly 1.8Å ; when both salt bridges between the interfacial band and pore oscillator are formed, the WT receptor has a minimum pore radius of at least 2.5Å.

The effects of the mutation on purely electrostatic barriers for chloride ion translocation was quantified via the Poisson-Boltzmann equation as described in SI Methods. The mutation from a positively charged to neutral residue led to insignificant changes in the electrostatic potential along the most favorable path given identical starting conformations (as shown in Supplementary Figure S12), suggesting that the mutation alone could not affect conductance without inducing conformational shift. Although the electrostatic potential is weakened near the mutation, the ion can adjust its pathway through the channel to fall closer to the other four residues in the interfacial band. Calculation of the electrostatic potential using the equilibrated structures of WT and K289M receptors showed a 5-10 kcal/mol (Figure S12C) higher electrostatic barrier in K289M, predominantly occurring in the transmembrane domain enclosing the residues containing the minimum pore constriction region.

The PMF for chloride ion translocation at 315K, measured using ABF, is shown in Figure 5. The largest barrier for the WT of 8 kcal/mol is proximal to the leucine residues at M2 9', forming the tightest constriction; this barrier is increased by 5 kcal/mol for the mutant

receptors. The difference in PMF near residue γ_2 289 is much less than 1 kcal/mol. While mutation of a positively charged to neutral residue does have a small effect on affinity of the chloride ion for the region of the receptor near the mutation, the dominant effect of the mutation on conduction is via conformational instability of the open state.

CONCLUSION

The primary new insights of this work are:

1. Repulsive cross-pore electrostatic interactions at the TMD-ECD interface (the “interfacial band”) stabilize the open state of the GABA(A) receptor; the interfacial band becomes more resistant to shrinking as the average separation between adjacent charges decreases or as the relative strength of diagonal interactions is reduced.
2. In GABA_{AR} receptors with 2 α subunits, 2 β subunits, and 1 γ subunit, a three-body charge-dipole arrangement (the “pore oscillator”) among three M2 helices (two adjacent and one diagonal) drives fluctuations in minimum pore radius, by alternating between a repulsive and an attractive configuration. All three charges are conserved within α , β and γ species of the GABA(A) receptor (although γ_3 has an arginine instead of a lysine, Figure S3).
3. Switching from an asymmetric to symmetric configuration of the interfacial residues in (1) can lock the charge-dipole interaction in (2) in a repulsive configuration, via a pair of salt-bridges between the pore oscillator and interfacial band.
4. Neutralizing one of the residues from (1), as in the epilepsy-associated γ_2 K289M mutations, makes the cost to shrink the interfacial band more sensitive to dispersion of the remaining charges; at higher temperatures this results in a significant population of closed states. This is consistent with the flickering observed in receptors with this

mutation in *vitro*, as well as the critical role of fever in inducing seizures for this phenotype.

The debate over the mechanism through which binding of a ligand at one site regulates the effects of binding of a ligand at another site (“allostery”) is over fifty years old,^{23,24} and much of that debate was focused on placing mechanisms within two extreme cases : ”conformational selection” (functional conformations are visited in the absence of ligand but stabilized by ligand, the Monod-Wyman-Changeux or MWC model) or ”induced fit” (functional conformations require all ligands to be bound, also known as the Koshland-Nemethy-Filmer model).

The mechanism for pore opening observed here fits most consistently with an MWC model, but the presence of both the interfacial band (1) and the pore oscillator (2) suggests a sequence of conformational events, with each event in the sequence falling at a different location along the continuum between pure conformational selection and pure induced fit. Although effects of the substitutions of interfacial band residues have been studied numerous times, we are unaware of mutagenesis studies involving either of the residues of the pore oscillator ($\gamma K/R285$ and $\beta E270$). The present simulation results suggest a role for these residues in determining receptor kinetics, including desensitization.

Our results indicate that a topological view of pLGICs may be counterproductive for conceptualizing gating mechanisms, because interactions entirely within a helix/subunit (or between two adjacent helices/subunits) are only indirectly related to conformation of the pore. While we present these results in heteropentamers, and the presence of the pore oscillator requires multiple subunit species, the role of symmetry in stabilizing conformations with open or occluded pores has been demonstrated previously in both heteropentamers such as nAChR⁴⁹ and homopentamers such as GLIC.⁵⁰ Our results indicate a critical role for diagonal interactions in determining the effects of asymmetry; asymmetry that decreases or increases diagonal distances opens or closes the pore respectively.

More generally, the Coulomb interaction between two charges placed on the diagonal of

a regular pentagon will only be moderately reduced from the interaction they would have as adjacent charges. Diagonal interactions will always contribute 38% of the overall interaction energy. A role for long range interactions within the nAChR TMD-ECD interface has been recently demonstrated by Auerbach and colleagues.⁵¹ The residues forming an interfacial band need not be located in the M2-M3 loop; they could also be in the M1 linker as in nAChR, or even in the M4 C-terminus. The concept of an interfacial band that we propose here is topologically abstract, but depends on pentameric symmetry and a regular charge density at the interface between the two domains; it may therefore be generalizable to many or even all pLGICs.

ACKNOWLEDGMENTS

SM, RS, and GB were supported by research grants NSF MCB1330728 and NIH P01GM55876-14A1. This project was supported with computational resources from the National Science Foundation XSEDE program through allocation NSF-MCB110149 as well as a local cluster funded by NSF-DBI1126052. The authors are grateful to Dr. Jérôme Hénin for multiple useful discussions.

References

- (1) Sigel, E. *Trends in Pharmacological Sciences* **1997**, *18*, 425–429.
- (2) Krasowski, M. D.; Harrison, N. L. *Cell. Mol. Life Sci.* **1999**, *55*, 1278–1303.
- (3) Harris, R. A.; Mihic, S. J.; Dildy-Mayfield, J. E.; Machu, T. K. *FASEB J* **1995**, *9*, 1454–1462.
- (4) Miller, K. W. *Br. J. Anaesth.* **2002**, *89*, 17–31.
- (5) Miller, P. S.; Aricescu, A. R. *Nature* **2014**, *512*, 270–275.

- (6) Hassaine, G.; Deluz, C.; Grasso, L.; Wyss, R.; Tol, M. B.; Hovius, R.; Graff, A.; Stahlberg, H.; Tomizaki, T.; Desmyter, A.; Moreau, C.; Li, X.-D.; Poitevin, F.; Vogel, H.; Nury, H. *Nature* **2014**, *512*, 276–281.
- (7) Du, J.; Lü, W.; Wu, S.; Cheng, Y.; Gouaux, E. *Nature* **2015**, *526*, 224.
- (8) Hilf, R. J. C.; Dutzler, R. *Nature* **2008**, *452*, 375–379.
- (9) Bocquet, N.; Nury, H.; Baaden, M.; Poupon, C. L.; Changeux, J.-P.; Delarue, M.; Corringer, P.-J. *Nature* **2009**, *457*, 111–114.
- (10) Gonzalez-Gutierrez, G.; Cuello, L. G.; Nair, S. K.; Grosman, C. *Proceedings of the National Academy of Sciences* **2013**, *110*, 18716–18721.
- (11) Sauguet, L.; Shahsavari, A.; Poitevin, F.; Huon, C.; Menny, A.; Nemecz, Á.; Haouz, A.; Changeux, J.-P.; Corringer, P.-J.; Delarue, M. *Proceedings of the National Academy of Sciences* **2014**, *111*, 966–971.
- (12) Hibbs, R. E.; Gouaux, E. *Nature* **2011**, *474*, 54–60.
- (13) Althoff, T.; Hibbs, R. E.; Banerjee, S.; Gouaux, E. *Nature* **2014**, *512*, 333.
- (14) Spurny, R. Ramerstorfer, J. Price, K. Brams, M. Ernst, M. Nury, H. Verheij, M. Legrand, P., Bertrand, D. Bertrand, S. Dougherty, D.A. De Esch, I.J.P. Corringer, P. Sieghart, W., Lummis, S.C.R. Ulens, C. *Proc.Natl.Acad.Sci.USA* **2012**, *109*, E3028.
- (15) Brannigan, G.; Hénin, J.; Law, R.; Eckenhoff, R.; Klein, M. L. *Proc. Natl. Acad. Sci. USA* **2008**, *105*, 14418–14423.
- (16) Willenbring, D.; Liu, L.; Mowrey, D.; Xu, Y.; Tang, P. *Biophys. J.* **2011**, *101*, 1905–1912.
- (17) LeBard, D. N.; Hénin, J.; Eckenhoff, R. G.; Klein, M. L.; Brannigan, G. *PLoS computational biology* **2012**, *8*, e1002532.

- (18) Yoluk, O.; Brömstrup, T.; Bertaccini, E. J.; Trudell, J. R.; Lindahl, E. *Biophys J* **2013**, *105*, 640–647.
- (19) Nury, H.; Bocquet, N.; Le Poupon, C.; Raynal, B.; Haouz, A.; Corringer, P.-J.; Delarue, M. *Journal of molecular biology* **2010**, *395*, 1114–27.
- (20) Zhu, F.; Hummer, G. *Proceedings of the National Academy of Sciences of the United States of America* **2010**, *107*, 19814–9.
- (21) Calimet, N.; Simoes, M.; Changeux, J.-P.; Karplus, M.; Taly, A.; Cecchini, M. *Proceedings of the National Academy of Sciences* **2013**, *110*, E3987–E3996.
- (22) Lev, B.; Murail, S.; Poitevin, F.; Cromer, B. A.; Baaden, M.; Delarue, M.; Allen, T. W. *Proceedings of the National Academy of Sciences* **2017**, *114*, E4158–E4167.
- (23) Changeux, J.-P.; Edelstein, S. *F1000 biology reports* **2011**, *3*.
- (24) Changeux, J.-P.; Christopoulos, A. *Cell* **2016**, *166*, 1084–1102.
- (25) Campos-Caro, a.; Sala, S.; Ballesta, J. J.; Vicente-Agulló, F.; Criado, M.; Sala, F. *Proceedings of the National Academy of Sciences of the United States of America* **1996**, *93*, 6118–23.
- (26) Grosman, C.; Salamone, F. N.; Sine, S. M.; Auerbach, A. *The Journal of general physiology* **2000**, *116*, 327–40.
- (27) Lummis, S. C. R.; Beene, D. L.; Lee, L. W.; Lester, H. A.; Broadhurst, R. W.; Dougherty, D. A. *Nature* **2005**, *438*, 248–52.
- (28) Lee, W. Y.; Sine, S. M. *Nature* **2005**, *438*, 243–7.
- (29) Unwin, N. *J. Mol. Biol.* **2005**, *346*, 967–989.
- (30) Lee, W. Y.; Free, C. R.; Sine, S. M. *The Journal of neuroscience : the official journal of the Society for Neuroscience* **2009**, *29*, 3189–99.

- (31) Sigel, ErwinBuhr, AndreasBaur, R. *Journal of Neurochemistry*. Oct99 **1999**, 73.
- (32) O'Shea, S. M.; Harrison, N. L. *The Journal of biological chemistry* **2000**, 275, 22764–8.
- (33) Kash, T. L.; Jenkins, A.; Kelley, J. C.; Trudell, J. R.; Harrison, N. L. *Nature* **2003**, 421, 272–5.
- (34) Hales, T. G.; Deeb, T. Z.; Tang, H.; Bollan, K. a.; King, D. P.; Johnson, S. J.; Connolly, C. N. *The Journal of biological chemistry* **2006**, 281, 17034–43.
- (35) Jaiteh, M.; Taly, A.; Hénin, J. *PloS one* **2016**, 11, e0151934.
- (36) Macdonald, R. *The Journal of physiology* **2010**,
- (37) Baulac, S.; Huberfeld, G.; Gourfinkel-An, I.; Mitropoulou, G.; Beranger, a.; Prud'homme, J. F.; Baulac, M.; Brice, a.; Bruzzone, R.; LeGuern, E. *Nature genetics* **2001**, 28, 46–8.
- (38) Bianchi, M.; Song, L. *The Journal of ...* **2002**, 22, 5321–5327.
- (39) Ramakrishnan, L.; Hess, G. P. *Biochemistry* **2004**, 43, 7534–40.
- (40) Eugène, E.; Depienne, C.; Baulac, S.; Baulac, M.; Fritschy, J. M.; Le Guern, E.; Miles, R.; Poncer, J. C. *The Journal of neuroscience : the official journal of the Society for Neuroscience* **2007**, 27, 14108–16.
- (41) Macdonald, R. L.; Kang, J.-Q.; Gallagher, M. J.; Feng, H.-J. *Adv Pharmacol* **2006**, 54, 147–169.
- (42) Kang, J.-Q.; Shen, W.; Macdonald, R. L. *The Journal of neuroscience : the official journal of the Society for Neuroscience* **2006**, 26, 2590–7.
- (43) Hénin, J.; Salari, R.; Murlidaran, S.; Brannigan, G.; Biology, I. *Biophysical journal* **2014**, 106, 1938–49.

- (44) Hibbs, R. E.; Gouaux, E. *Nature* **2011**, *474*, 54–60.
- (45) MacKerell, A. D. et al. *The journal of physical chemistry. B* **1998**, *102*, 3586–616.
- (46) Klauda, J. B.; Venable, R. M.; Freites, J. A.; O'Connor, J. W.; Tobias, D. J.; Mondragon-Ramirez, C.; Vorobyov, I.; MacKerell, A. D.; Pastor, R. W. *The journal of physical chemistry. B* **2010**, *114*, 7830–43.
- (47) Pitman, M. C.; Suits, F.; Mackerell, A. D.; Feller, S. E. *Biochemistry* **2004**, *43*, 15318–28.
- (48) Phillips, J. C.; Braun, R.; Wang, W.; Gumbart, J.; Tajkhorshid, E.; Villa, E.; Chipot, C.; Skeel, R. D.; Kalé, L.; Schulten, K. *Journal of computational chemistry* **2005**, *26*, 1781–802.
- (49) Mitra, A.; Cymes, G. D.; Auerbach, A. *Proceedings of the National Academy of Sciences* **2005**, *102*, 15069–15074.
- (50) Mowrey, D.; Cheng, M. H.; Liu, L. T.; Willenbring, D.; Lu, X.; Wymore, T.; Xu, Y.; Tang, P. *Journal of the American Chemical Society* **2013**, *135*, 2172–2180.
- (51) Gupta, S.; Chakraborty, S.; Vij, R.; Auerbach, A. *The Journal of General Physiology* **2017**, *149*, 85–103.

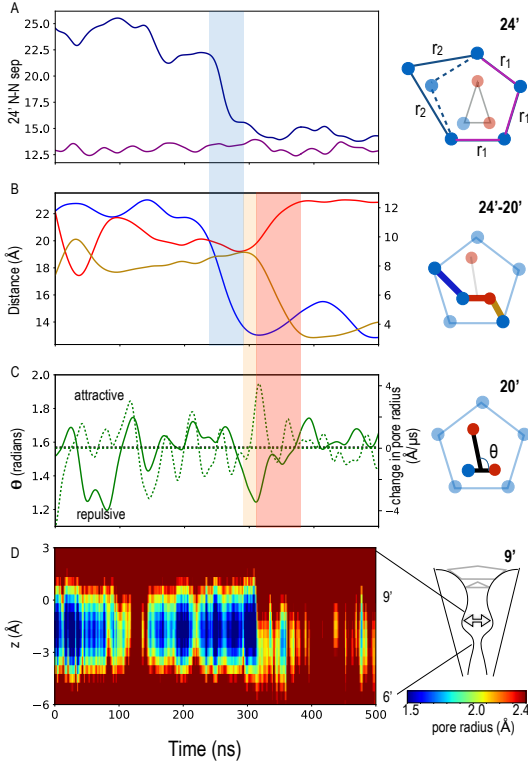


Figure 2: Evolution of the interfacial band and pore oscillator in one replica of the WT system at 315K. (A) Flip of one residue (α -K279) so the interfacial band switches from elongated to regular pentamer, occurs at ~ 250 ns, followed by a series of events leading to the pore opening between ~ 250 ns - 350 ns, as marked by the shaded regions. (B) The distances between residues α K279 – γ K285, plotted on y-axis and γ K285 – β -K270, β -K270 – β -K274, plotted on alternate y-axis, are shown in blue, red and gold respectively. (C) The solid green curve depicts the angle between the charge-dipole arrangement representing the pore oscillator ; The Dotted green line represents the pore-opening event as measured by calculating the first derivative of the minimum pore radius. (D) Pore radius as a function of distance along the pore axis and time. All curves are smoothed as described in SI Methods. Transition windows are shaded blue (early), orange (mid), and red (late).

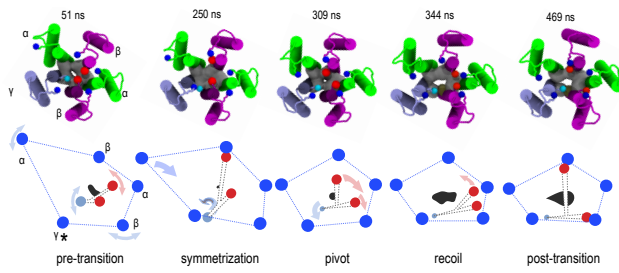


Figure 3: Evolution of pore oscillator and interfacial band during spontaneous opening event. Top: Representative frames are shown from the WT trajectory at 315K, with coloring as in Figure 1B/C. Bottom: Cartoon of transition highlighting movement of the charged groups forming interfacial band(blue) and pore oscillator (γ K280-cyan, β E270-red). Dashed lines connecting the points of the pore oscillator and interfacial band are for visualization purposes only and do not represent physical bonds. The filled gray shape indicates the unoccluded area of the hydrophobic gate. After α K279 flips during the symmetrization step, M2 helices separate along the axis connecting the flipped and current positions (frame at 344 ns), while after the acidic residues pivot, M2 helices separate along the axis connecting the two acidic residues (post-transition panel). Salt-bridges are represented by contacting red and blue spheres. The asterisk marks the charge that is neutralized with the K289M mutation.

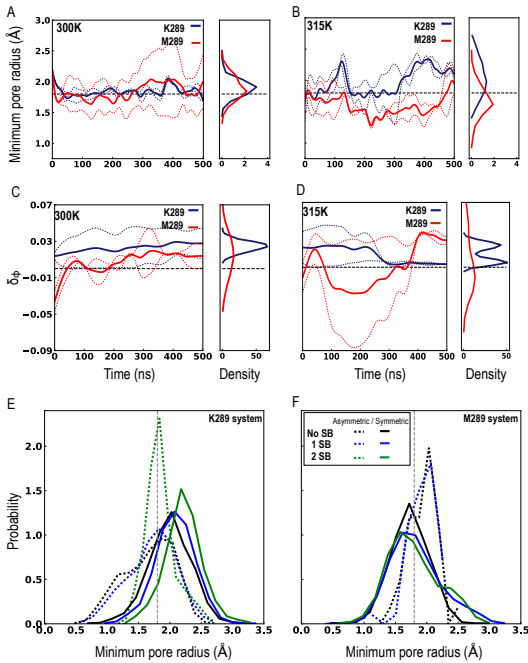


Figure 4: Correlations between shape of interfacial band, pore radius, and salt-bridging between interfacial band and pore oscillator for multiple replicas and temperatures. (A/B) Smoothed time evolution of the pore minimum constriction, averaged (solid lines) over two replicas (shown separately as dotted lines) each, at 300 K and 315 K. The radius of a chloride ion is represented by the dashed horizontal line at 1.8 Å. (C/D) Smoothed time evolution and distribution of δ_ϕ for both WT and K289M systems at 300 and 315 K. Distribution trends are similar to those generated numerically, discussed in SI Theory. (E/F) Distribution of minimum constriction radius for conformations clustered by total number of β K274-E270 salt-bridges and symmetrization of the interfacial band.

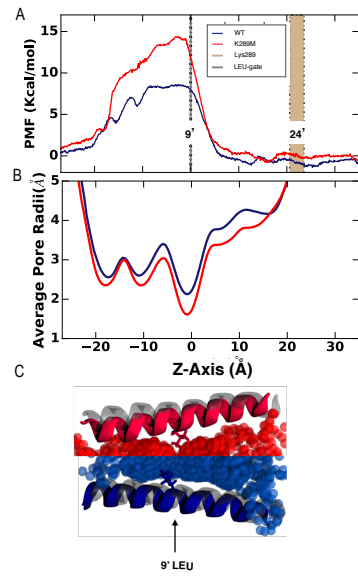


Figure 5: (A) Potential of mean force profile of a chloride ion crossing the ion channel, calculated at 315K for a receptor that remained primarily in the elongated conformation for the WT and had a flexible interfacial band for the K289M. The full PMF including the rest of the simulation box is in Fig S14. (B) Average pore radius profile for the conformations in (C).